Twins and their boundaries during homoepitaxy on Ir(111)

Sebastian Bleikamp,[1] Johann Coraux,[1,2,*] Odile Robach,[3] Gilles Renaud,[3] and Thomas Michely[1]
[1]*II Physikalisches Institut, Universität zu Köln, D-50937 Köln, Germany*
[2]*Institut Néel, CNRS-UJF, 25 Rue des Martyrs, B.P. 166, F-38042 Grenoble Cedex 9, France*
[3]*Commissariat à l'Energie Atomique, Institut Nanosciences et Cryogénie, 17 Avenue des Martyrs, F-38054 Grenoble Cedex 9, France*
(Received 9 June 2010; revised manuscript received 10 November 2010; published 14 February 2011)

The growth and annealing behavior of strongly twinned homoepitaxial films on Ir(111) have been investigated by scanning tunneling microscopy, low-energy electron diffraction, and surface x-ray diffraction. *In situ* surface x-ray diffraction during and after film growth turned out to be an efficient tool for the determination of twin fractions in multilayer films and to unravel the nature of lateral twin crystallite boundaries. The annealing of the twin structures is shown to take place in a two-step process; first, the length of the lateral twin crystallite boundaries is reduced, without affecting the amount of twinned material, and then, at much higher temperatures, the twins themselves anneal. Within moderately annealed films lateral twin crystallite boundaries are visible at the film surface as fractional steps from which strain fields extend. The nature of these boundaries is discussed.

DOI: 10.1103/PhysRevB.83.064103 PACS number(s): 61.72.Nn, 61.72.Mm, 68.37.Ef, 61.72.Dd

I. INTRODUCTION

Stacking faults are known to seriously affect the properties of thin films and devices. The local change of stacking sequence may, for instance, modify the magnetic properties of thin films.[1,2] Stacking faults are also known to act as electron scattering planes in metal nanowires,[3] to act as traps for electrons in SiC,[4,5] and to limit the performance of optoelectronic III–V nanowire-based devices.[6]

A single stacking fault on a plane normal to the growth direction initiates the growth of a twin crystallite. The fault plane is also termed the coherent twin boundary or twin plane (see Fig. 1). It is a coherent grain boundary with an extremely low energy. This low energy is the reason why twin crystallites nucleate easily and why they are among the most frequent defects in thin films.[7] Upon continued growth the twin crystallite becomes embedded in the crystalline matrix and develops also lateral boundaries, that is, boundaries more or less parallel to the growth direction. Due to the mismatch of atomic positioning at lateral twin crystallite boundaries, they possess considerable boundary energies.

In epitaxy often regular and twinned crystallites nucleate with equal probability at the substrate interface, for example, for a face-centered cubic (fcc) deposit on a (0001) surface of a hexagonal compact substrate.[8] In such situations regular and twinned crystallites are in fact equivalent and were therefore termed double positioning structures, giving rise to double positioning boundaries (see Fig. 1). Double positioning boundaries were first observed by Dickson and Pashley in Au films on mica by transmission electron microscopy (TEM)[9] and subsequently the subject of intense research.[7,8,10–13] Specifically, the double positioning boundaries in Au films were found to have a strong tendency to be aligned along $\langle 1\bar{1}0\rangle$ directions, to be normal to the film surface plane, to move in a thermally activated fashion, and even to disappear for liquid-like films in the nucleation stage.[12] In the grain boundary language, double positioning boundaries in an fcc metal aligned along the $\langle 1\bar{1}0\rangle$ directions belong to the class of $\Sigma 3$ $\langle 1\bar{1}0\rangle$ tilt boundaries, that is, every third atom is found on a coincidence site lattice.[14–18]

Here we investigate homoepitaxial films on Ir(111). In a homoepitaxial system no stacking faults should be present due to energetics. Complications due to chemical inhomogeneities or epitaxial strain are absent. Despite the high stacking fault energy for Ir we found significant stacking fault nucleation probabilities on Ir(111) and explained this and the proliferation of faults in atomistic detail.[19–23] The homoepitaxial situation is more complex compared to heteroepitaxial growth, as twin crystallites do not just nucleate at the substrate. Twin formation occurs in different layers, which gives rise to an additional type of lateral boundary separating two twins of different stacking sequence,[21] rather than a twin and a regular crystallite (see Fig. 1). Also, these boundaries are lateral twin crystallite boundaries, as they separate two differently stacked twin crystallites, but to distinguish them from double positioning boundaries separating a twin crystallite from the regular matrix, we refer to them as stacking boundaries.

In distinction to previous studies, we combine here the surface view of growth of a twinned film obtained by low-energy electron diffraction (LEED) and scanning tunneling microscopy (STM) with the surface + subsurface view provided by surface x-ray diffraction (SXRD). Our tools allow us to follow twinning during growth in a quantitative way, and this already at low temperatures where twin structures are rather complex and the lateral twin crystallite boundaries are disordered. We are able to monitor the evolution of the twin plane extension and of the lateral twin crystallite boundaries as a function of temperature over an extended range from 300 to 1600 K and to obtain insight into their structure, temperature-dependent reorganization, and strain. Two interesting observations are the presence of fractional surface steps caused by double positioning boundaries and the formation of twins with respect to {111} planes other than the (111) substrate one.

II. EXPERIMENTAL PROCEDURE

The STM and LEED experiments were performed in a UHV system with a base pressure below 5×10^{-11} mbar.

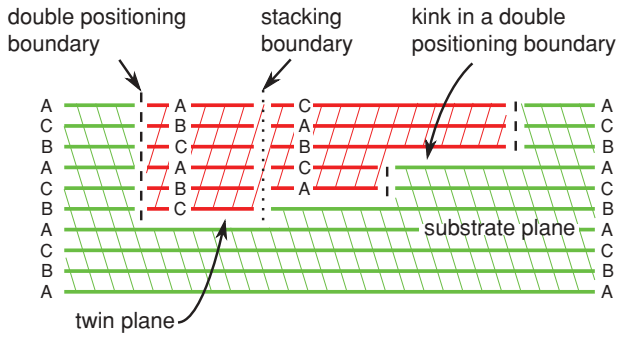

FIG. 1. (Color online) Schematics of a cross section of crystallites grown at the surface of an fcc(111) substrate. Regular, untwinned crystallites appear as a stacking of green (light-gray) planes following an ABC sequence (left-inclined lines); twinned crystallites appear as a stacking of red (dark-gray) planes following a CBA sequence (right-inclined lines). Two types of lateral twin crystallite boundaries are shown: double positioning boundaries (dashed lines), separating crystallites that are 180° twinned one with respect to the other, as well as a stacking boundary (dotted line; see text for definition). A kink is also considered at one of the double positioning boundaries.

The sample was cleaned by repeated cycles of sputtering with 1.5-keV Xe^+ or Ar^+ ions at 1100 K and annealing to 1600 K. Iridium was deposited from a current-heated Ir wire with a standard deposition rate of 1.3×10^{-2} ML/s, where 1 ML (monolayer) is the surface atomic density of Ir(111). Imaging was performed with a home-built, magnetically stabilized STM.[24] Unless otherwise specified, all images are differentiated and appear as illuminated from the left. The topographs were digitally postprocessed with the WSxM software.[25] For the LEED I/V analysis, a rear-view camera LEED system was used.

SXRD experiments were performed at the SUV instrument[26,27] installed at the BM32 beamline of the European Synchrotron Radiation Facility (ESRF), in a UHV system coupled to a *Z*-axis diffractometer and with a base pressure below 3×10^{-10} mbar. Sample preparation and deposition in this UHV system followed the same procedure as for the STM and LEED experiments. A monochromatic 18-keV photon beam incident under an angle of 0.273° with respect to the surface was used. The corresponding x-ray attenuation length for Ir is 51 Å[28] (23 ML). Note that this is an average value because the sample surface had a bowing of 0.2°, resulting in a spread of incidence angles. The incident beam was doubly focused to a size of 0.3×0.2 mm^2 (full width at half-maximum in horizontal and vertical directions, respectively) at the sample location. Detector slits, located 570 mm away from the sample, were set at 2 mm parallel to the sample surface (which was vertical) and 2.2 mm perpendicular to it (with 5-mm guard slits at 200 mm), resulting in an angular acceptance of 0.2° in both directions.

For the general description of planes and directions, the standard cubic system is used ($a_{Ir} = 3.8392$ Å). The surface plane is indicated by (111) and the corresponding direction by [111]; lateral facets of the same symmetry but not parallel to the surface are indicated by {111}, and the corresponding directions as ⟨111⟩.

III. STM EXPERIMENTS

Figures 2(a)–2(d) display characteristic elements of a homoepitaxial growth sequence on Ir(111) discussed in more detail previously.[21,22] After deposition of 0.2 ML as in Fig. 2(a) dendritic single atom high islands are visible. They display a triangular envelope due to the preferred formation of {111}-microfaceted step edges. The triangular shape of the island in the image center is mirrored (or rotated by 180°) in orientation. This mirrored orientation marks stacking fault islands with the atoms residing in the threefold coordinated hollow sites corresponding to an hexagonal compact rather than an fcc stacking sequence. Continued deposition gives rise to island coalescence, and most stacking fault islands switch to regular stacking during this process.[20] At the boundary between regular and remaining faulted areas, narrow stripes of

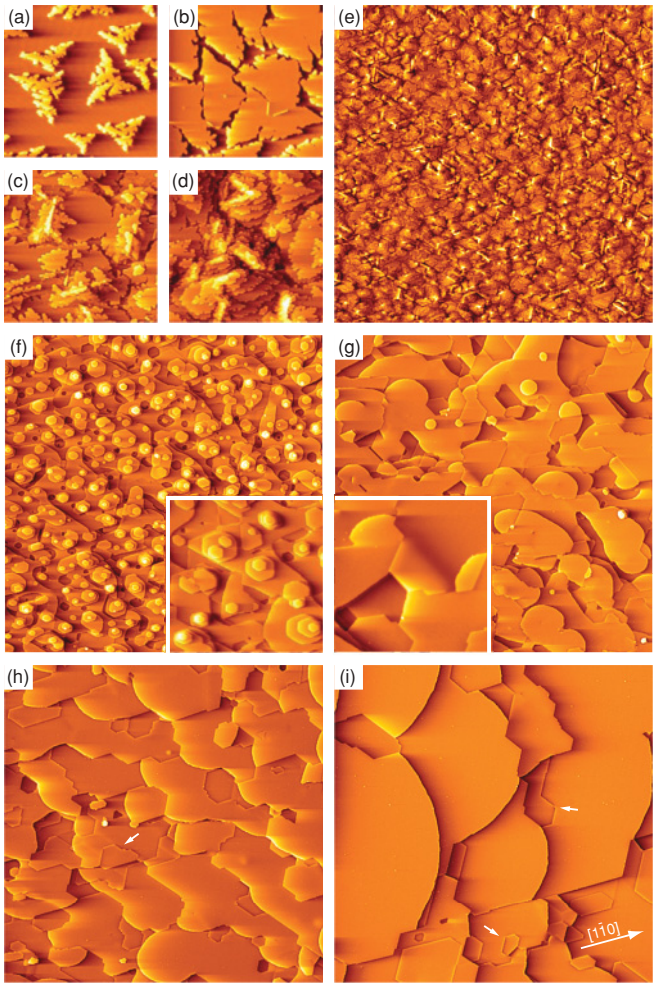

FIG. 2. (Color online) (a–d) STM topographs illustrating characteristic features at different stages of homoepitaxy on Ir(111) after deposition of (a) 0.2 ML, (b) 0.9 ML, (c) 10 ML, and (d) 90 ML at 350 K. (e) Larger-scale STM topograph of a 90-ML film grown at 350 K. (f–i) STM topographs of the film shown in (e) after successive 180-s annealing steps at (f) 850 K, (g) 1025 K, (h) 1200 K, and (i) 1375 K. Image size: (a–d) 64 × 64 nm; (e–i) 480 × 480 nm; insets in (f) and (g), 120 × 120 and 67 × 67 nm, respectively. Small white arrows in (h) and (i) indicate the surface trace of emerging screw dislocation lines (junctions between up-and-down steps).

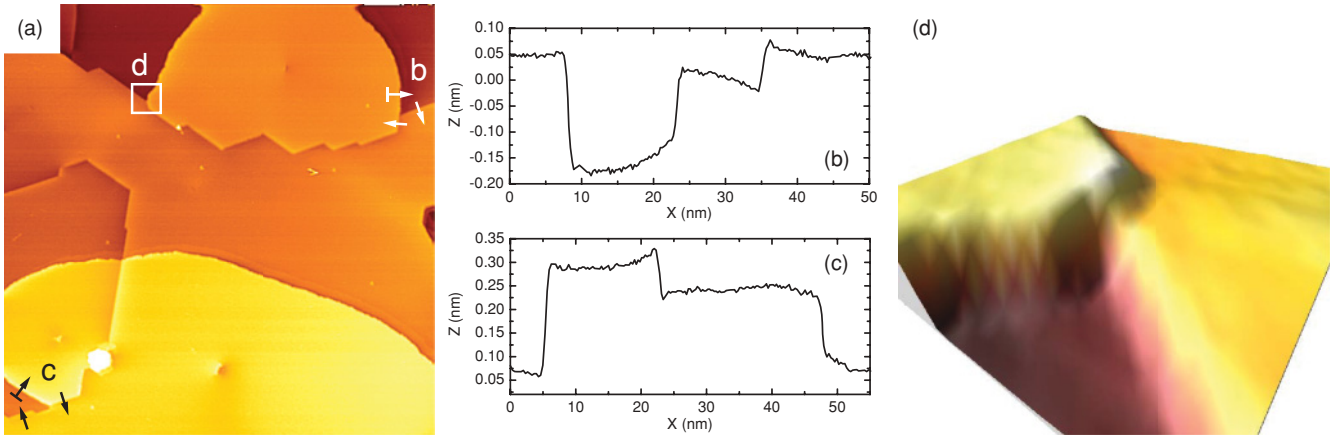

FIG. 3. (Color online) (a) Grayscale STM topograph after deposition of a 90-ML film at 350 K and additional annealing to 1025 K for 180 s. Image size: 128 × 128 nm. (b, c) Line scans along paths indicated in (a) illustrating full and fractional step heights as well as strain fields associated with fractional steps. (d) Three-dimensional visualization of the junction marked in (a).

subatomic width are present, which offer fourfold coordinated adsorption sites. This gap and thus also the faulted area bounding on one of its sides become stabilized by adatoms forming a monatomic width decoration row oriented along $\langle 1\bar{1}0\rangle$ [Fig. 2(b)]. Continued growth takes place preferentially by heterogeneous nucleation at these decoration rows. The heterogeneous nucleation prevents formation of additional faults on top of the initial one and, thereby, ensures twin crystallite growth. Moreover, it also induces twin crystallite growth in its surroundings with the stacking fault (twin plane) one layer above the initial fault. This results in additional twins separated from the initial one by a stacking boundary.[21,22] In Fig. 2(c) the situation after 10 ML deposited is shown, where overgrown decoration rows mark the separation of differently stacked surface areas. Eventually, further deposition gives rise to an irregular rough surface dominated by mounds. They result from heterogeneous nucleation at the boundaries between differently stacked areas of the films [compare Fig. 2(d)].

The same film is shown in Fig. 2(e) in a demagnified view. Each of the bright features marks a $\langle 1\bar{1}0\rangle$ oriented lateral twin crystallite boundary. In an annealing sequence with successive annealing intervals of 180 s this rough and heavily twinned film is subsequently heated to higher and higher temperatures. In Fig. 2(f) after annealing to 850 K the film has become much smoother and the typical structure size has increased. Decoration rows or bright features oriented along $\langle 1\bar{1}0\rangle$ are now absent. After annealing to 1025 K [Fig. 2(g)] the film is very flat and the characteristic structure size is further increased. Straight steps precisely oriented along the $\langle 1\bar{1}0\rangle$ directions are visible. These straight steps have heights of only a fraction of a regular monatomic step. In addition, curved steps of monatomic height are visible. They are pinned where they touch fractional steps. The monatomic steps are invariably curved outward toward the downhill side. The outward curvature appears to imply an enhanced surface chemical potential, which for the case of Fig. 2(g) may be traced back to decaying adatom islands also visible. The inset in Fig. 2(g) highlights a terrace smoothly bent around a $\langle 1\bar{1}0\rangle$ axis. Such step-free bending of terraces prevails up to the highest annealing temperatures. We tentatively attribute these bent terraces to buried defects that give rise to the fractional steps at the surface (discussion later). The last two annealing steps, to 1200 K [Fig. 2(h)] and 1375 K [Fig. 2(i)], increase the typical structure size further, that is, the step density decreases. The distinction between rounded monatomic steps and straight steps of fractional height is obvious. The fact that even in Fig. 2(i), after the decay of all adatom islands, pinned monatomic steps are invariably curved outward is possibly caused by less strongly bound atoms in the defect structures associated with the fractional steps.

Figure 3(a) shows a height image (not differentiated) of an area with straight (fractional) and curved (monatomic) steps in detail. Example line scans around the junction points marked with the arrows in Fig. 3(a) are shown in Figs. 3(b) and 3(c). The situation at a typical triple junction is depicted in a three-dimensional view in Fig. 3(d). Neglecting, for the moment, heavily distorted areas, only three kinds of steps are found: (i) steps with a height of 2.2 ± 0.2 Å, corresponding to the (111) layer distance (2.22 Å); (ii) steps with a height of 0.75 ± 0.1 Å, that is, steps that display, within the limits of error, a fractional height of one-third of a monatomic step; and (iii) steps with a height of 1.5 ± 0.3 Å, that is, steps that display, within the limits of error, a fractional height of two-thirds of a monatomic step [compare Figs. 3(b) and 3(c)]. The measured step heights do not depend on the tunneling voltage and are thus a topographic effect. Evidently, fractional steps cannot be present on the (111) surface of a perfect Ir crystal and their occurrence proves the presence of extended defect structures in the Ir film even after annealing to 1375 K [compare Fig. 2(i)]. In the vicinity of the fractional steps, typically an upward (downward) bending of the upper (lower) terrace perpendicular to the step direction takes places. It extends over a distance of about 9 nm, with significant scatter, and indicates the presence of strain next to the fractional steps.

A postdecoration technique was employed to assess the stacking of the surface areas of the Ir films after annealing.[29] Ir, 0.1–0.2 ML, was deposited on the annealed film surface at room temperature. Dendritic Ir islands with the characteristic triangular envelope grow; they display the same orientation in

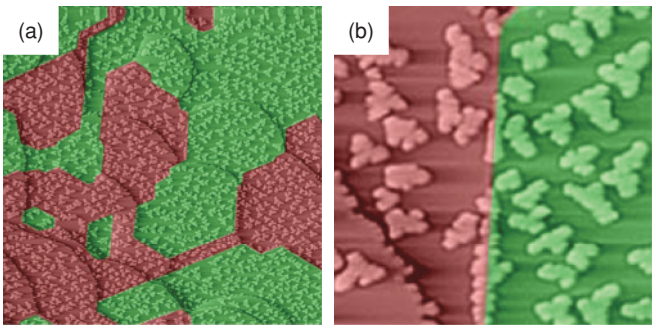

FIG. 4. (Color online) STM topographs after deposition of 90 ML at 350 K, subsequent annealing to 1200 K for 180 s, and final 0.2 ML Ir deposition at room temperature. The predominant orientation of the triangular envelope of the small dendritic islands allows one to identify the regular crystal matrix and twin crystallites, appearing in green (light gray) and red (dark gray), respectively. Image sizes: (a) 255 × 255 nm and (b) 44 × 44 nm.

an area of uniform stacking, with a preference of about 90%. Areas of mirrored stacking display consequently mirrored preferences of the triangular island envelopes. Application of the postdecoration method to the surface after annealing at 1200 K is exemplified in Fig. 4. The areas are marked depending on the stacking sequence identified. We find that even after annealing to 1200 K, more than 50% of the surface area of the 90-ML films is twinned with respect to the bulk crystal. This result is backed up by quantitative LEED I/V analysis[22] and further supported in this article by quantitative analysis of SXRD measurements, which are sensitive to the stacking of the film grains over their full thickness.

As illustrated in Fig. 4 twinned and untwinned surface areas are always separated by fractional steps precisely oriented along the $\langle 1\bar{1}0\rangle$ directions. Thus the fractional steps are the surface trace of lateral twin crystallite boundaries, of double positioning or $\langle 1\bar{1}0\rangle$ tilt grain boundaries. We find twin areas to consist of perfect terraces without defects other than monatomic steps. Therefore we conclude that stacking boundaries are absent after annealing to 1200 K. As the surface topography at 1025 K is qualitatively identical to the one at 1200 K [compare Fig. 2(g) with Fig. 2(h)], we conclude that stacking boundaries are already annealed even at 1025 K.

We note that fractional steps analyzed in previous STM work are distinct from the ones found here, as they were found within areas of identical stacking.[30–32] To obtain additional information on the dynamic behavior of these defects and for complementary subsurface information, we performed SXRD experiments.

IV. SXRD EXPERIMENTS

Figure 5(a) displays the reciprocal lattice of an fcc crystal cut in the plane perpendicular to the [111] direction (green circles) and containing the $[\bar{2}11]$ direction. For a truncated crystal, the loss of symmetry in direct space creates a reciprocal lattice of crystal truncation rods [CTRs; solid lines in Fig. 5(a)] perpendicular to the surface and connecting the reciprocal lattice points corresponding to the bulk crystal.[33] Accordingly, the main intensity maxima coincide with the bulk reflections. We now consider Ir homoepitaxial growth. As we have shown

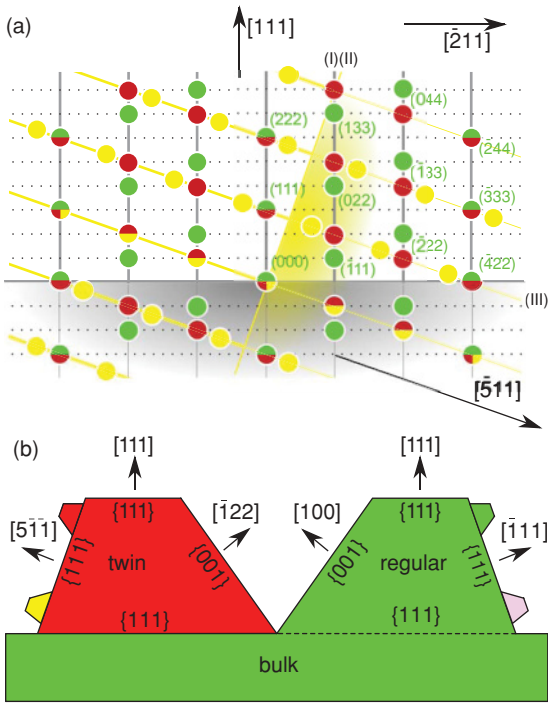

FIG. 5. (Color online) (a) Reciprocal space cut in the plane defined by the [111] and $[\bar{2}11]$ directions of an fcc crystal. Green (medium-gray) circles depict the reciprocal lattice of the regular crystal; red (dark-gray) circles depict the reciprocal lattice of a twin crystal, that is, of a regular crystal rotated by 180° around the [111] axis; yellow (light-gray) circles depict the reciprocal lattice of this twinned crystal, but additionally rotated by 180° around the $[\bar{5}11]$ direction of the initial regular crystal (twin-of-twin) that matches the $[\bar{1}11]$ direction of the twin crystal. For multitwin peaks, half- or quarter-circles are employed. Shaded areas represent truncated crystals: the gray crystal is terminated by a (111) surface, while the yellow (light gray) one corresponds to the $(\bar{1}11)$ termination of the twin, that is, a $(\bar{5}11)$ surface in the frame of reference of the initial crystal. These truncated crystals produce CTRs that are displayed as solid gray or yellow (light-gray) lines. (b) Cross section depicting the facets and the corresponding orientations with respect to the regular crystal matrix. On the left (right) facet of the twin (regular) crystallite are shown two small crystallites, one with the same structure as the initial twin crystallite that is displayed with the same color, and one whose structure is twinned with respect to the initial twin crystallite. The latter two are the twin-of-twin and the twin and are shown in yellow and violet, respectively (light grays).

previously,[19–23] the overgrowing Ir may either prolong regular bulk stacking or grow after the introduction of a stacking fault as a twin crystallite, that is, a crystal portion rotated by 180° around the [111] axis [Fig. 5(b)]. The regular stacking contributes to the CTR intensities of the substrate. The twin crystallite gives rise to a reciprocal lattice rotated by 180° around [111]. As an illustration, for the CTR passing through $1/3(\bar{4}22)$ [labeled (I) in Fig. 5(a)], intensity maxima at $(\bar{1}11)$, (022), (133), etc., corresponding to the bulk (green circles), are supplemented by maxima shifted by 1/3[111], corresponding to the twin (red circles). Monitoring the relative twin and regular intensities along the CTRs during growth qualitatively provides information on the relative twin/regular fraction.[34] Due to the non-negligible probing depth, for the initial growth

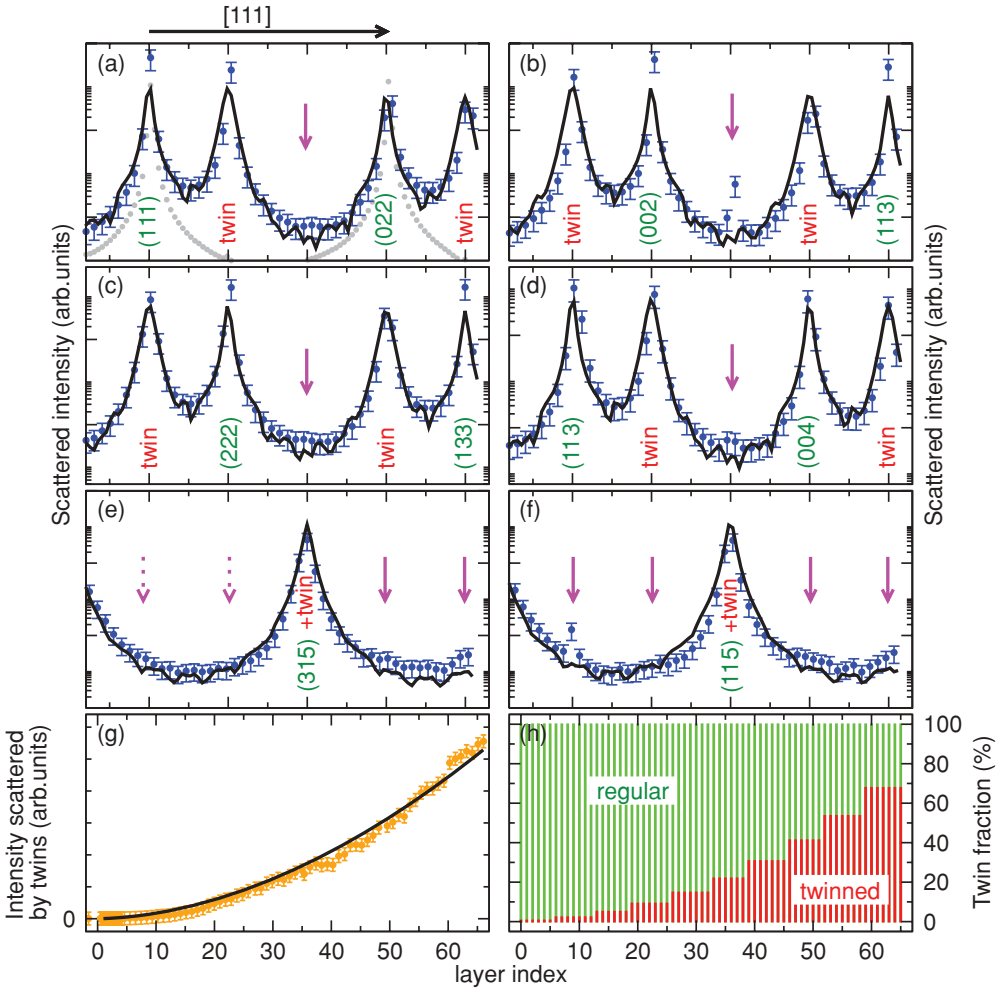

FIG. 6. (Color online) (a–f) Integrated intensity scattered along six CTRs perpendicular to the (111) surface, that is, along the [111] direction, after deposition of 68 ML Ir on Ir(111) at 350 K. Filled circles represent the data, while solid lines correspond to the fit of the whole set of CTRs. (a) and (c) correspond to the CTRs marked (I) and (II) in Fig. 5(a). Bragg reflections for the regular untwinned crystal are indicated in green (light gray). Positions for the twinned crystal are labeled "twin." Vertical arrows point to positions where faint extra contributions are observed. The data set displayed in gray in (a) is the integrated scattered intensity for the substrate prior to the growth of the Ir thin film. (g) Integrated intensity at the left position marked "twin" in (b), as a function of the deposited amount. The dots represent the data, the solid line was computed through the parameters from the fit of the CTRs. (h) Fraction of twin regions in the Ir film as a function of the layer index, as deduced from the fit of the CTRs.

stages the x-ray signal is dominated by the bulk signal. As extensively shown in the literature for a single or a few layer deposits only, a careful analysis accounting for interferences between the twinned and the untwinned regions allows one to quantitatively determine the stacking composition in these layers. Here we show that such a quantitative analysis can also be performed for much thicker films ($\simeq$70 atomic layers).

Figures 6(a)–6(f) show the x-ray scattered intensity along a set of six CTRs, all of them along the [111] direction [Figs. 6(a) and 6(c) are the CTRs marked (I) and (II) in Fig. 5(a); the others could be sketched in other appropriate cuts in reciprocal space], after deposition of 68 ML of Ir at 350 K. The occurrence and location of strong maxima different from the bulk reflections along four of the CTRs [Figs. 6(a)–6(d)], together with the absence of extra maxima along the two others [Figs. 6(e) and 6(f)], are an unambiguous signature for a large twin fraction in the Ir thin film. In between the Bragg peaks, the intensity variations correspond to the roughness only for Fig. 6(e) and to a mixture of the roughness contribution and of the twin signal for Figs. 6(a) and 6(c). The Bragg peaks for the substrate [on the gray curve in Fig. 6(a)] are narrower than those for the fcc regions in the thin films, confirming that the x-ray beam probes prominently the top region of the sample, where the effective lateral extension of the regular domains is reduced—compared to the bare substrate—due to the presence of twin domains. The appearance of the twin signal was monitored *in situ* during growth by measuring the integrated intensity around the left position marked "twin" in Fig. 6(b). The result is shown in Fig. 6(g), where a smooth increase is observed starting from 0. Note that, in contrast to the STM analysis, this evolution takes into account not only the fraction of twins at the topmost layer, but also the twins in the layers below, as a result of the penetration depth of x rays. In addition to the typical twin signals, fainter extra features are also observed

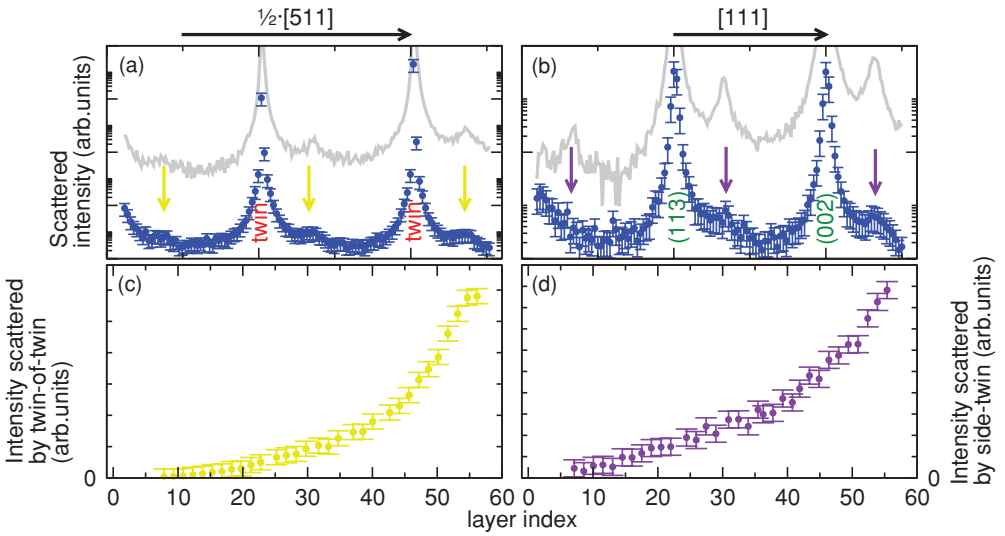

FIG. 7. (Color online) (a, b) Intensity scattered along lines in the $[5\bar{1}\bar{1}]$ (a) and $[11\bar{1}]$ (b) directions, after deposition of 68 ML Ir on Ir(111) at 350 K. (a) Corresponds to CTRs marked (III) in Fig. 5(a). In (a) Bragg reflections for the twinned crystal are labeled "twin"; in (b) those for the untwinned crystal are shown in green (gray). Vertical arrows point to positions of the twins-of-twins (a) and of the side-twins (b), which are better visible for scans (gray lines; shifted upward for clarity) corresponding to the scattered intensity after annealing at 750 K. The intensity measured off the peaks is a mixture between the lateral facet $[(5\bar{1}\bar{1})$ and $(11\bar{1})]$ signals and that from the corresponding stacking faults. (c, d) Intensity at the central position marked by a vertical arrow in (a) and (b) as a function of the Ir deposit (see text).

along the CTRs. These features are marked by vertical arrows in Figs. 6(a)–6(d). Some of them are very faint; two of them are barely visible. Their observation, though very sensitive to the alignment of the goniometer axis, is confirmed in a second series of experiments. Their origin is discussed later.

The quantitative analysis of the Ir film composition was performed by using a simple model detailed in Sec. I of Ref. 35, allowing us to simulate the scattered intensity along the whole set of CTRs with a single set of parameters that are refined by a least squares minimization algorithm. Through this procedure we obtained the thin-film stacking composition in terms of the twin fraction as a function of the film height. As displayed in Fig. 6(h) the model finds a twin fraction of 70% at the surface, which agrees, within the limits of uncertainties, with the STM data presented here. We obtained an rms roughness of 4.3 Å (see Sec. I of Ref. 35), in rough agreement with the STM analysis resulting in 2.5 Å.

The large amount of time needed for the measurement of a full set of CTRs prevented us from doing such a measurement during the growth of the thin film. As an alternative, we measured the integrated intensities below a twin peak and below a regular peak over a restricted range in reciprocal space during growth [Fig. 6(g)]. These intensities provide *a priori* only a qualitative characterization of the evolution of the amount of twins. However, comparison of these scattered intensities to the ones calculated within the Ir growth model in which the stacking composition follows the quantitative picture developed here provides quantitative insight. The calculations nicely reproduce the data as shown in Fig. 6(g). The evolution displayed in Fig. 6(g) may then be interpreted by inspection of our model [Fig. 6(h)]. After deposition of about 10 ML the twin fraction becomes noticeable and increases more and more rapidly. We know from STM experiments[36] that after 10 ML the growth mode changes from layer-by-layer growth to rough growth dominated by heterogeneous nucleation at decoration rows [cf. Fig. 2(c)] with rapid proliferation of stacking faults.

We then explored the stacking sequences on the lateral facets of regular and twin Ir crystallites, that is, on their {111} facets other than (111) (for twin crystallites these are {115} planes if expressed in the regular fcc frame), and the possible appearance of new Ir orientations corresponding to twinning with these inclined facets as twin planes [Fig. 5(b)]. This leads to six new possible twin-daughter orientations of Ir, three from the regular parent and three from the (111)-twin parent. Accordingly, we explored lines in reciprocal space being perpendicular to the {111} and {115} planes, respectively. Figure 7(a) shows the integrated scattered intensity along the line marked (III) in Fig. 5(a), that is, along the $[5\bar{1}\bar{1}]$ direction, which is normal to a {111} plane of a twin crystallite. In addition to the expected twin peaks, new ones develop, as highlighted by the vertical arrows and better visible on the gray curve obtained after annealing. The intensity of such peaks was monitored during growth [Fig. 7(c)]. These new peaks are generated by twin daughters of the (111)-twin parent (twin-of-twin), as shown in Figs. 5(a) and 5(b). A similar observation is made along a line lying perpendicular to a $(11\bar{1})$ plane [Figs. 7(b) and 7(d)]: the regular reflections are supplemented by extra features developing during growth that are generated by one of the twin daughters of the regular parent (side-twin), more precisely the one resulting from a 180° rotation around the $[11\bar{1}]$ direction.

V. TEMPERATURE DEPENDENCE

Figure 8 compares the annealing temperature dependence of the twin fraction estimated by different techniques. The black squares in Fig. 8(a) display the fraction of twinned

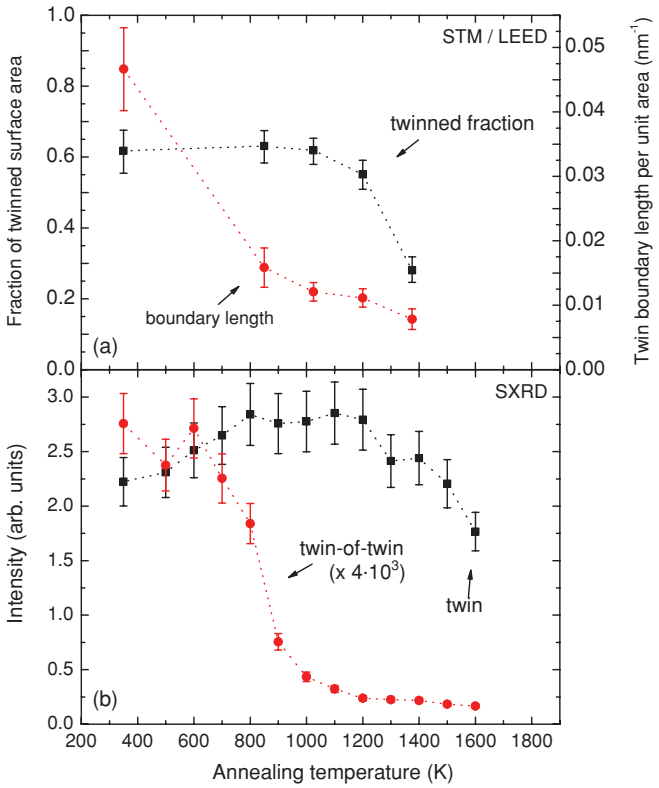

FIG. 8. (Color online) (a) Fraction of twinned surface area measured by LEED (filled squares) and lateral twin crystallite boundary length measured by STM (filled circles) for a 90-ML Ir film grown on Ir(111) at 350 K, as a function of the annealing temperature. (b) The x-ray scattered intensity from twins [filled squares; measured at the left position marked "twin" in Fig. 6(b)] and from twins-of-twins [filled circles; measured at the central location marked with a vertical arrow in Fig. 7(a)] as a function of the annealing temperature.

surface area as a function of the annealing temperature measured by LEED. It is about 0.6 up to 1025 K, then gradually drops, but does not vanish even for the highest annealing temperature, 1400 K. The integrated x-ray intensity around the left position marked "twin" in Fig. 6(b), shown in Fig. 8(b) as black squares, is also indicative of twinning with respect to the (111) surface plane. It measures not only the surface area but also the average twin fraction in the film volume underneath the surface due to the integration depth of SXRD. The amount of twinning apparently does not change up to an annealing temperature of 1200 K and only then gradually decreases. Roughly, both data sets agree that (i) twins start to decay in the temperature range of 1000 to 1200 K and (ii) even the highest annealing temperature used is not sufficient to remove them entirely. We attribute the shift in the onset of twin annealing toward higher temperatures in the x-ray data to the higher pressure during Ir thin-film deposition. In LEED annealing sequences we noticed that this onset depends sensitively on the pressure during deposition. Most likely it is related to a higher amount of carbon containing residual gas, which partly decomposes on the surface during growth. This results in incorporation of carbidic species into the film, which may hinder twin annealing at higher temperatures.

The filled (red) circles in Fig. 8(a) show the length of the lateral twin crystallite boundaries as obtained by STM. At low temperatures the boundary length is derived from grooves, decoration rows, and ridges in mounds elongated along ⟨110⟩, and at high temperatures, from the length of the fractional steps. The lateral twin crystallite boundary length decreases rapidly upon annealing at temperatures that are well below the onset temperature for a decrease in the twinned surface area [filled black squares in Fig. 8(a)].

Filled red dots in Fig. 8(b) measure the x-ray intensity at the central position marked by a vertical arrow in Fig. 7(a) during annealing, that is, for twins on a {111} lateral facet of a twinned crystallite. The measured intensity displays a similar temperature dependence as the boundary length measured by STM. It decreases already around 700 K, at much lower temperatures than the twin intensity itself. We therefore tentatively conclude that the *twin-of-twin* intensity is linked to the lateral twin crystallite boundaries.

VI. DISCUSSION

We first discuss the annealing behavior of defective Ir thin films. The reduction in the lateral twin boundary length as measured by STM and displayed in Fig. 8(a) needs to be complemented by an analysis of the nature of the boundaries present dependent on temperature. At 350 K the boundary length is derived from decoration rows and ridges in the topography. As discussed in detail in Ref. 22 (cf. Fig. 2 here and Fig. 11 in Ref. 22), ridges and decoration rows indicate not only double positioning boundaries but also stacking boundaries. After annealing the films to elevated temperatures the only defects that can be associated with grain boundaries are the fractional steps. Using our decoration technique we demonstrated in Fig. 4 that the fractional steps are exclusively double positioning boundaries separating twins from the regular matrix. Stacking boundaries are entirely absent. The decrease in lateral twin crystallite boundary length by about a factor of 3, from 350 to 850 K can thus be attributed to the complete annealing of the stacking boundaries. Neighboring twins of different stacking sequences, originating from their different depths of formation, merge efficiently to a single twin. Stacking boundaries thus either are of very high energy (large driving force for annealing) or possess a high mobility.

There seems to be a second contribution to lateral twin crystallite boundary length reduction. According to Fig. 8(a) the decrease in twin crystallite boundary length at elevated temperatures cannot be explained entirely by a loss of twin area. We assume a reshaping of twinned areas, making them more compact. Thereby the ratio of twin area to double positioning boundary length would decrease as observed. Reshaping of twinned areas can also contribute to the initial strong decrease in twin crystallite boundary length up to 850 K.

Based on our SXRD and LEED data shown in Fig. 8, the twin area and volume decrease when the annealing temperature reaches about half the melting temperature of Ir (2739 K). At such temperatures usually the equilibrium concentration of bulk vacancies increases sharply, thereby opening a pathway for bulk diffusion. However, we note that we were never able to remove twins entirely from our crystal after growth of films

with thickness of the order of 100 ML just by annealing. To restore the crystal, extensive removal of material by sputtering was necessary.

The strong decrease in the twin-of-twin SXRD signal in Fig. 8 up to 900 K makes it plausible that the twins-of-twins are located at the lateral twin crystallite boundaries, most likely at the stacking boundaries. As shown in Fig. 11 in Ref. 22, at 350 K the formation of neighboring twins in different layers, and thus with different stacking sequences, involves the formation of {111} lateral facets of one of the twinned crystallites. The disordered and strained region between the two twins of different stacking could well be the feed for the nucleation of a twin-of-twin on such a {111} facet of a twin crytallite. The simultaneous disappearance of the SXRD twin-of-twin signal and of the stacking boundaries is then a logical consequence. Nevertheless, twins-of-twins may also be partly present at double positioning boundaries, which also bear considerable strain. We note that Kong *et al.* observed a large number of stacking faults to be present in double positioning boundaries of β-SiC,[8] an observation that could be related to our twin-of-twin finding.

Next we discuss the presence of bent terraces without steps. As pointed out in the pioneering work of Jacobs and Stowell,[11] a double positioning boundary may also have a kink; that is, instead of going straight from the substrate to the film surface, it is cut into two parts connected in the interior of the film by a twin plane (see Fig. 1 here and Fig. 1 in Ref. 11). As a double positioning boundary involves a displacement of the two crystallites by a fraction (here one-third) of an atomic layer, a bent terrace observed in STM could well result from the strain field of such a kink in a double positioning boundary.

Finally, we address the question after the atomic structure of double positioning boundaries. As already pointed out, these boundaries are of the $\Sigma 3$ type $\langle 1\bar{1}0\rangle$ tilt boundaries, a type of boundary that has been extensively investigated. Figure 9(a) sketches a few possible low-index crystal plane combinations: {112}/{112}-, {001}/{122}-, and {111}/{115}-type boundaries. From energetic considerations, for a film of given thickness h the boundary with the minimum value of the product $\gamma h \cos\vartheta$ will be selected. Here γ is the specific grain boundary energy, and ϑ the angle between the substrate normal and the grain boundary plane. Recent atomistic simulations for Cu and Al indicate that $\gamma h \cos\vartheta$ has a minimum for the symmetric {112}/{112} grain boundary.[18] Although γ is rather high for this grain boundary, the geometric factor $h \cos\vartheta$ overcompensates this. Also, one of our observations is in favor of symmetric {112}/{112} grain boundaries. Experimentally we observe no difference in the morphology of opposing fractional steps enclosing a twin (or regular crystallite). As illustrated in Figs. 9(b) and 9(c), the {112}/{112} boundary is the only one that is identical for regular-twin and twin-regular grain boundaries. Asymmetric grain boundaries would differ for the two cases. Finally, Pashley and Stowell also find, in their early TEM observations for Au films on mica, a strong preference for {112}/{112} grain boundaries as double positioning boundaries.

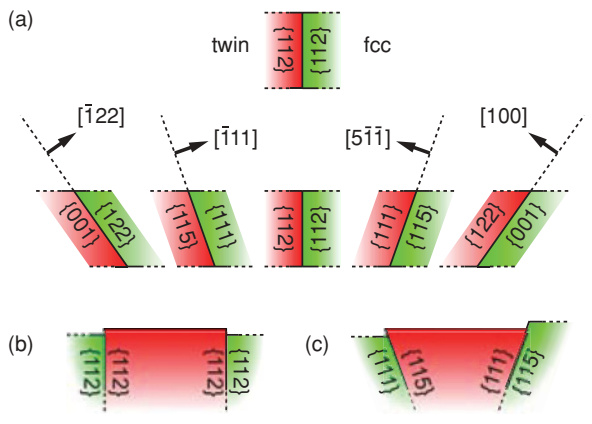

FIG. 9. (Color online) (a) Models of possible double positioning boundaries involving low-index planes. Twin crystallites, shown in red (dark gray), are embedded in an untwinned matrix, shown in green (light gray), with (b) {112}/{112} and (c) {111}/{115} twin boundaries.

Assuming the {112}/{112} boundary to be the double positioning boundary in our films, the question comes up whether this type of boundary is consistent with the observed fractional steps of one-third and two-thirds height. The answer is yes, but not definitively. In the literature it was found that the energetically preferred shift of the two crystallites depends on the material, on the thickness, and on the size of the boundary. Shifts of 1/2 {111} plane spacing were found for Au.[37] For the paradigmatic case of Al there is a consensus that, for boundaries that are not too small, the shifts are about one-third (or, equivalently, two-thirds) of a lattice spacing (compare the discussions in Refs. 38 and 39). To our best knowledge, for Ir neither experiments nor calculations exist for any $\Sigma 3$ $\langle 1\bar{1}0\rangle$ tilt boundary. Therefore, the observed fractional step heights of one-third and two-thirds are consistent with the {112}/{112} boundary as the double positioning boundary in Ir thin films, given our present knowledge. The strain fields extending away from the fractional steps are nothing but expected if one takes into account that the crystallites are both connected to the substrate. Similar strain fields have been calculated and were observed experimentally.[39]

In support of our view of one-third fractional step heights we simulated the X-ray scattered intensity in three dimensions, for a system consisting of two crystallites, one untwinned, and the other twinned. Details of the calculation are given in Sec. II of Ref. 35. Two situations were considered: (i) the (111) net planes of the two crystallites are not shifted with respect to each other; and (ii) the (111) net planes of the two crystallites are shifted by one-third net plane separation with respect to each other. The calculation along the reciprocal space plane defined by [111] and [$\bar{1}\bar{1}$2] is shown in Figs. 10(a) and 10(b) for (i) and (ii), respectively. The most obvious difference between the two maps is the appearance of one horizontal line (gray arrow in Fig. 10) along which constructive interferences yield increased intensity. The horizontal feature intersects all [111]-CTRs, including also those scanned in Figs. 6(b) and 6(d) [marked (IV) and (V), respectively, in Fig. 10]. It is worth noting here that the intensity is not much increased right at the intersection between (IV), (V), and the horizontal feature. However, if, due to some small misalignment, the CTRs are scanned a little off their exact position, the extra feature will become better pronounced. Due to limited goniometer alignment, this is shown in Figs. 6(b) and 6(d) to a certain

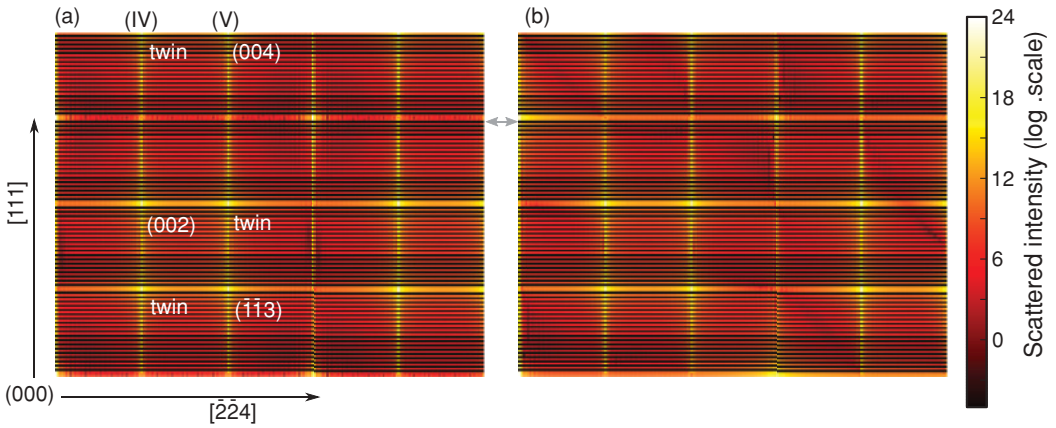

FIG. 10. (Color online) Intensity map for a {112}/{112} boundary between an untwinned and a twinned crystal of the same size, (a) without and (b) with a shift in the $(11\bar{1})$ lateral facet resulting in a height difference of one-third monolayer (see text). The fringes are due to the finite size of the crystallites considered for the calculation.

extent. Similar features were reproduced as well for all other cuts of the reciprocal space relevant to the CTRs scanned in Figs. 6(a)–6(d). The extra features observed on the CTRs are thus presumably generated by the one-third net plane shifts and therefore correspond to the one-third and two-thirds steps.

VII. CONCLUSION AND SUMMARY

Homoepitaxial growth on Ir(111) at 350 K is characterized by a proliferation of twins leading to an areal fraction of twin approaching 70% for about 70 ML, as determined by SXRD and STM. We find that by successive annealing steps to higher and higher temperatures, first the stacking boundaries disappear, which separate neighboring twins of different stacking sequence. Then a twin reshaping proceeds, shortening the double positioning boundaries, and eventually the twin crystallite volume starts to diminish. However, it turned out to be impossible to remove the twins entirely from films with a thickness of the order of 100 ML by annealing to two-thirds the melting temperature. SXRD finds unambiguous evidence for twins on {111} planes inclined toward the (111) substrate plane. Based on their moderate annealing temperature we attribute these twins-of-twins to be located at the stacking boundaries, a type of boundary of specific relevance in the homoepitaxy on Ir(111). STM finds one-third and two-thirds fractional steps visualizing double positioning boundaries in well-annealed films at the surface. Based on the appearance of these boundaries in STM, consistent with our SXRD simulations and the available literature, we attribute these boundaries to be symmetric $\Sigma 3$ $\langle 1\bar{1}0\rangle$ tilt boundaries, that is, of type {112}/{112} and normal to the film surface. Cross-sectional TEM of such boundaries could confirm this interpretation and provide additional insight into their atomic structure.

ACKNOWLEDGMENT

Support by the Deutsche Forschungsgemeinschaft through the project "Kinetics of Stacking Faults in Thin Films" is acknowledged.

*Corresponding author: johann.coraux@grenoble.cnrs.fr

[1] S. Krause, L. Berbil-Bautista, T. Hënke, F. Vonau, M. Bode, and R. Wiesendanger, Europhys. Lett. **76**, 637 (2006).
[2] L. Berbil-Bautista, S. Krause, M. Bode, and R. Wiesendanger, Phys. Rev. B. **76**, 064411 (2007).
[3] J. Wang, M. Tian, T. E. Mallouk, and M. H. W. Chan, J. Phys. Chem. B **108**, 841 (2004).
[4] H. Iwata, U. Lindefelt, S. Öberg, and P. R. Briddon, Phys. Rev. B **65**, 033203 (2001).
[5] U. Lindefelt, H. Iwata, S. Oberg, and P. R. Briddon, Phys. Rev. B **67**, 155204 (2003).
[6] J. Johansson, L. Karlsson, C. Svensson, T. Artensson, B. Wacaser, K. Deppert, L. Samuelson, and W. Seifert, Nature Mater. **5**(7), 574 (2006).
[7] M. J. Stowell, *Epitaxial Growth, Part b*, edited by J. W. Matthews (Academic Press, New York, 1975), p. 437.
[8] H. S. Kong, B. L. Jiang, J. T. Glass, G. A. Rozgonyi, and K. L. More, J. Appl. Phys. **63**, 2645 (1988).
[9] E. W. Dickson and P. W. Pashley, Phil. Mag. **7**, 1315 (1962).
[10] D. W. Pashley and M. J. Stowell, Phil. Mag. **8**, 1605 (1963).
[11] M. H. Jacobs and M. J. Stowell, Phil. Mag. **11**, 591 (1965).
[12] M. J. Stowell and T. J. Law, Phys. Status Solidi B **16**, 117 (1966).
[13] M. Nakamura, T. Isshiki, T. Nishiguchi, K. Nishio, S. Ohshima, and S. Nishino, Mater. Sci. Forum **483-485**, 181 (2005).
[14] R. C. Pond and V. Vitek, Proc. R. Soc. London A **357**, 453 (1977).
[15] J. M. Pénisson, U. Dahmen, and M. J. Mills, Phil. Mag. Lett. **64**, 277 (1991).
[16] U. Wolf, F. Ernst, T. Muschik, M. W. Finnis, and H. F. Fischmeister, Phil. Mag. A **66**, 991 (1992).
[17] K. L. Merkle and D. Wolf, Phil. Mag. A **65**, 513 (1992).
[18] M. A. Tschopp and D. L. McDowell, Phil. Mag. **87**, 3147 (2007).
[19] C. Busse, C. Polop, M. Müller, K. Albe, U. Linke, and T. Michely, Phys. Rev. Lett. **91**, 056103 (2003).
[20] C. Busse and T. Michely, Surf. Sci. **552**, 281 (2004).

[21]S. Bleikamp, A. Thoma, C. Polop, G. Pirug, U. Linke, and T. Michely, Phys. Rev. Lett. **96**, 115503 (2006).
[22]S. Bleikamp, A. Thoma, C. Polop, and T. Michely, Phys. Rev. B **77**, 245424 (2008).
[23]S. Bleikamp and T. Michely, Thin Solid Films **518**, 1914 (2009).
[24]T. Michely, M. Kaiser, and M. J. Rost, Rev. Sci. Instrum. **71**, 4461 (2000).
[25]I. Horcas, R. Fernandez, J. M. Gomez-Rodriguez, J. Colchero, J. Gomez-Herrero, and A. M. Baro, Rev. Sci. Instrum. **78**, 013705 (2007).
[26]R. Baudoing-Savois, M. D. Santis, M. C. Saint-Lager, P. Dolle, O. Geaymond, P. Taunier, P. Jeantet, J. P. Roux, G. Renaud, A. Barbier, O. Robach, O. Ulrich, A. Mougin, and G. Berard, Nucl. Instrum. Methods Phys. Res. Sect. B **149**, 213 (1999).
[27]R. Baudoing-Savois, G. Renaud, M. D. Santis, A. Barbier, O. Robach, P. Taunier, P. Jeantet, O. Ulrich, J. P. Roux, M. C. Saint-Lager, A. Barski, O. Geaymond, G. Berard, P. Dolle, M. Noblet, and A. Mougin, Nucl. Instrum. Methods Phys. Res. Sect. B **159**, 120 (1999).
[28]B. Henke, E. Gullikson, and J. Davis, At. Data Nucl. Data Tables **54**, 181 (1993).
[29]K. Meinel, M. Klaua, and H. Bethge, Phys. Stat. Sol. A **110**, 189 (1988).
[30]H. F. Wolf and H. Ibach, Appl. Phys. A **52**, 218 (1991).
[31]E. Lundgren, B. Stanka, M. Schmid, and P. Varga, Phys. Rev. B **62**, 2843 (2000).
[32]J. Christiansen, K. Morgenstern, J. Schitz, K. Jacobsen, K.-F. Braun, K.-H. Rieder, E. Lgsgaard, and F. Besenbacher, Phys. Rev. Lett. **88**, 206106 (2002).
[33]I. K. Robinson, Phys. Rev. B **33**, 3830 (1986).
[34]J. Camarero, J. de la Figuera, J. J. de Miguel, R. Miranda, J. Álvarez, and S. Ferrer, Surf. Sci. **459**, 191 (2000).
[35]See supplemental material at [http://link.aps.org/supplemental/10.1103/PhysRevB.83.064103].
[36]This is also observed in the SXRD data; namely, the integrated intensity measured in anti-Bragg position displays ML oscillations (not shown here), consistent with layer-by-layer growth, up to 10 ML.
[37]E. A. Marquis, D. L. Medlin, and F. Léonard, Acta Mater. **55**, 5917 (2007).
[38]A. F. Wright and S. R. Atlas, Phys. Rev. B **50**, 15248 (1994).
[39]J. C. Hamilton and S. M. Foiles, Phys. Rev. B **65**, 064104 (2002).